

## Field Emission from $V_2O_5 \cdot nH_2O$ Nanorod Arrays

Wen Chen,\* Chiwei Zhou, Liqiang Mai, Yueli Liu, Yanyuan Qi, and Ying Dai

State Key Laboratory of Advanced Technology for Materials Synthesis and Processing, and Institute of Materials Science and Engineering, Wuhan University of Technology, Wuhan, 430070, China

Received: August 17, 2007; In Final Form: December 3, 2007

Hydrated vanadium pentoxide ( $V_2O_5 \cdot nH_2O$ ) nanorod arrays with diameters of  $\sim 200$  nm and lengths of more than  $5 \mu m$  have been synthesized via template-based physical wetting of  $V_2O_5$  sols. The  $V_2O_5 \cdot nH_2O$  nanorod arrays were characterized by scanning electron microscopy, X-ray diffraction, and high-resolution transmission electron microscopy. Field-emission (FE) measurements on the  $V_2O_5 \cdot nH_2O$  nanorod arrays show low turn-on voltages of  $6\text{--}8$  V/ $\mu m$  and linear Fowler–Nordheim behaviors. The morphologies and natures of the  $V_2O_5 \cdot nH_2O$  samples are assumed to cause such good FE performances.

### Introduction

Field-emission (FE) devices based on microfabrication Mo tips are commercially available, but researchers are actively looking for alternative materials. Generally, the materials used as FE emitters would be very thin and made of conductors or semiconductors with high mechanical strength, as well as being inexpensive and easy to process. Among the materials, carbon nanotubes (CNTs) are studied extensively because of their high aspect ratios and unique electrical and mechanical properties. However, it is still difficult to control their FE behaviors, and their exact FE mechanism is not well understood.

In the present work, we attempt to look for alternative materials to serve as FE emitters. Due to their semiconductor characteristics, the oxides of transition metals have the advantage of a lower surface potential barrier than that of metals, which is beneficial to electron FE properties.<sup>1</sup> Among these metal oxides,  $V_2O_5$  makes an attractive choice because of the multiple valence state of vanadium and its band gap of not more than 2.9 eV.<sup>2</sup> Nevertheless, to our knowledge, no FE data on  $V_2O_5$  nanorod arrays have been reported up to now.

Recently, great attention has been focused on the synthesis and applications of nanostructured materials, and one of the most dynamic research areas is on the synthesis of one-dimensional nanostructures, such as nanowires, nanorods, and nanotubes.<sup>3–5</sup> Various techniques have been established, and among them, template-based synthesis is one of the most common fabrication methods, particularly for mass production and alignment. In this method, a porous membrane, such as anodic alumina or polycarbonate (PC), is used as a template and precursor of the desired material. Filling of the template pores can be achieved by capillary forces,<sup>6,7</sup> electric field,<sup>8</sup> centrifugation force,<sup>9</sup> chemical vapor deposition,<sup>10</sup> and so forth. However, as for amphoteric oxide  $V_2O_5$ , the PC membrane and electric field are the most commonly used choice.<sup>11–13</sup> Cao's group did a lot of good and interesting work in using capillary forces for filling the pores.<sup>7,9,12,13</sup> Herein, we have fabricated  $V_2O_5$  nanorod arrays by utilizing capillary forces but adding the process of vacuum pumping, which can decrease the fabricating time. FE properties of the hydrated  $V_2O_5$

nanorod arrays before and after heat treatment and the relationship between the FE properties and nanostructures are discussed.

### Experimental Section

Aligned  $V_2O_5 \cdot nH_2O$  nanorods were fabricated via a simple route of template-based physical wetting of  $V_2O_5$  sols with two steps. The first step is  $V_2O_5$  sols preparation, prepared by reaction between  $H_2O_2$  and  $V_2O_5$  powder.<sup>14,15</sup> Here, 0.5 g of crystalline  $V_2O_5$  powder and 25 mL of  $H_2O_2$  (30%) were mixed in a flask (50 mL) with stirring in an ice bath. In the initial stage, due to the decomposition of  $H_2O_2$  and the formation of the vanadium peroxide complex ion, the oxygen was produced out of the solution with an exothermic reaction. After 20 min, the bright orange solution formed, and then, after up to 24 h, the red–brown  $V_2O_5$  sols were obtained. The second step is fabrication of  $V_2O_5 \cdot nH_2O$  nanorod arrays. Some  $V_2O_5$  sols were dropped on a cleaned glass slide substrate, and the dried PC membrane (Whatman, pore diameters of  $\sim 200$  nm, thickness of  $6\text{--}11 \mu m$ ) was put on the sols and attached well onto the substrate. At last, the sample was put into the vacuum drying oven and dried at  $70^\circ C$  for more than 24 h. The times of vacuum pumping were three times more. X-ray diffraction (XRD) was carried out on an X'Pert powder diffractometer (PANalytical, The Netherlands) with Cu  $K_\alpha$  radiation ( $\lambda = 1.5418 \text{ \AA}$ ) to investigate the phase structure of the products. The diffraction data were recorded for  $2\theta$  between  $5$  and  $60^\circ$ , with a resolution of  $0.033^\circ$ . Scanning electron microscopy (SEM) images were collected on a JSM-5610LV microscope operated at 20 kV to investigate the surface morphology of the as-grown sample after removing the PC template by pyrolysis and oxidation in air. High-resolution transmission electron microscopy (HRTEM) images were obtained through an IEM-2100F microscope (JEOL, Japan) at an accelerating voltage of 200 kV to further analyze the microstructure of the as-grown sample. The FE measurement was carried out in a vacuum chamber with a pressure greater than  $5 \times 10^{-7}$  Pa at room temperature under a two parallel plate configuration, and the distance between the sample and electrode was adjusted up to hundreds of micrometers. The emission current was measured using a Keithly 6485 picoammeter.

\* To whom correspondence should be addressed. E-mail: chenw@whut.edu.cn. Tel: +86-27 87651107. Fax: +86-27 87864580.

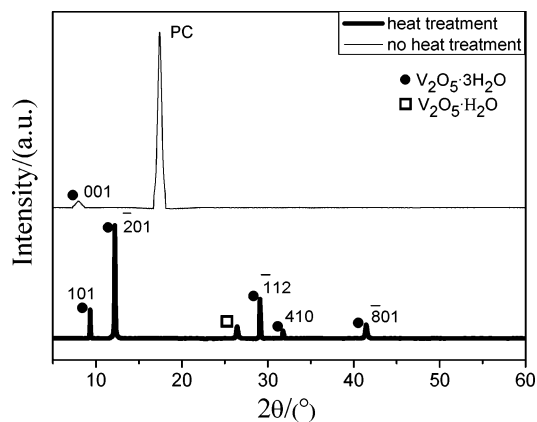


**Figure 1.** XRD patterns of the as-synthesized products before and after heat treatment.

## Results and Discussion

Figure 1 shows the XRD patterns of the as-grown products before and after heat treatment, which can be briefly described as having the PC membrane removed by being fired at 480 °C in air for 1 h through pyrolysis and oxidation.<sup>13</sup> It can be seen that there exists a peak at  $2\theta$  between 15 and 20°, which is attributed to the PC membrane.<sup>2</sup> Other peaks are observed at  $2\theta$  between 5 and 60° with  $2\theta$  values of 7.306, 9.33, 12.19, 29.09, 31.76, and 41.42°, which correspond to the (001), (101), (201), ( $\bar{1}12$ ), (410), and ( $\bar{8}01$ ) diffraction planes of the monoclinic  $V_2O_5 \cdot 3H_2O$  crystal [No. 7-332], respectively. A peak is also observed at the  $2\theta$  value of 26.41°, corresponding to an unknown  $V_2O_5 \cdot H_2O$  crystal [No. 21-1432]. By comparison, it can be found that after heat treatment, the peak of the PC membrane disappearing corresponds to the template being removed, and other peaks at  $2\theta$  between 9 and 45° appearing corresponds to the as-synthesized products changing from amorphous to crystalline vanadium oxide, which mainly consists of the monoclinic  $V_2O_5 \cdot 3H_2O$  crystal. The SEM image of the sample after heat treatment is shown in Figure 2a. From the image and its inset, which is another SEM image of the same sample, it can be revealed that the as-grown  $V_2O_5 \cdot nH_2O$  nanostructure has one-dimensional array morphology, covering the surface of the glass slide substrate. Also, it can be seen that the length of the nanorod is more than 5  $\mu\text{m}$ , which corresponds to the thickness of the PC membrane. Typical TEM images of single nanorods without and with heat treatment are shown in Figure 2c and e, respectively, from which the solid structure of the nanorods can be clearly recognized, and from that, it can be also seen that the diameters of the nanorods before and after heat treatment are about 251.40 and 163.73 nm, respectively, which are around 200 nm, corresponding to the diameters of the pores of the PC template. The diameters after heat treatment are smaller than the ones before heat treatment because of shrinkage and densification.<sup>16</sup> By comparison of TEM images and corresponding HRTEM images (Figure 2d and f) and fast Fourier transform (FFT) images (insets of Figure 2d and f), it can be clearly shown that the treatment results in the densification and crystallization of the as-prepared products. Before heat treatment, Figure 2c and d shows that the product is amorphous  $V_2O_5 \cdot nH_2O$ . However, after the treatment, Figure 2e and f indicates that the product is crystalline  $V_2O_5 \cdot nH_2O$  because it exhibits the well-defined lattice fringes with the lattice spacing measured at  $3.10 \pm 0.05 \text{ \AA}$ , which corresponds to the distance between the ( $\bar{1}12$ ) planes in monoclinic  $V_2O_5 \cdot 3H_2O$ . Furthermore, its corresponding FFT image confirms the nature of the  $V_2O_5 \cdot 3H_2O$  crystals in the as-prepared products. Energy

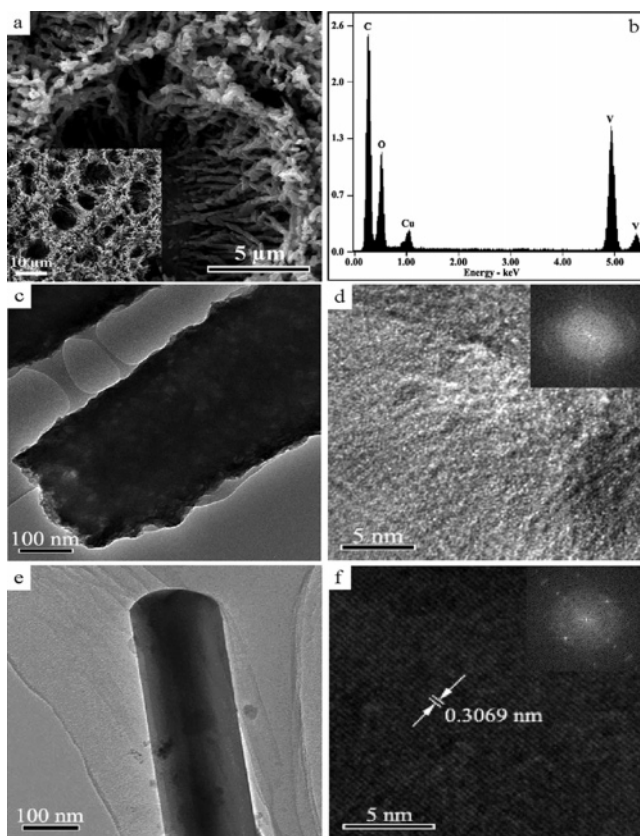


**Figure 2.** (a) Top view of SEM image of vanadium oxide nanoarrays (the inset is another image of the nanoarrays). (b) EDS pattern of the  $V_2O_5 \cdot nH_2O$  nanorods after heat treatment. (c) TEM image of an isolated  $V_2O_5 \cdot nH_2O$  nanorod before heat treatment. (d) HRTEM image of the  $V_2O_5 \cdot nH_2O$  nanorod before heat treatment (the inset is the corresponding FFT image). (e) TEM image of an isolated  $V_2O_5 \cdot nH_2O$  nanorod after heat treatment. (f) HRTEM image of the  $V_2O_5 \cdot nH_2O$  nanorod after heat treatment (the inset is the corresponding FFT image).

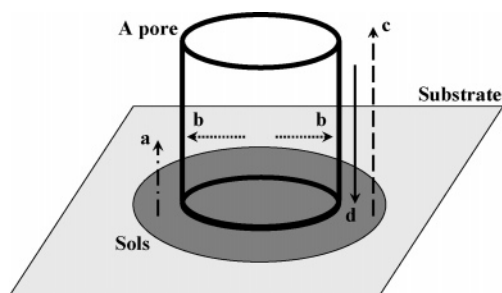


**Figure 3.** This schematic demonstrates the different acting forces of the growth process: (a) capillary force, (b) coulomb force, (c) effect of negative pressure, and (d) gravity action. It is under these combined forces that  $V_2O_5 \cdot nH_2O$  nanoarrays have formed.

dispersive spectroscopy (EDS) pattern of the nanorods (Figure 2b) confirms the vanadium oxide composition of the as-synthesized products.

Figure 3 is a schematic drawing of the different acting forces of the growth process. It demonstrates the main forces that we believe occur in the growth process. Therefore, the formation mechanism of the  $V_2O_5 \cdot nH_2O$  nanorod arrays can be described as follow: (a) a capillary force because of the nanometer pores of the PC membrane, good for the formation; (b) a coulomb force due to the electronegativity of pore walls<sup>17</sup> and the electropositivity<sup>18</sup> of the sols, also benefiting the formation; (c) the effect of negative pressure, the key force for the growth;

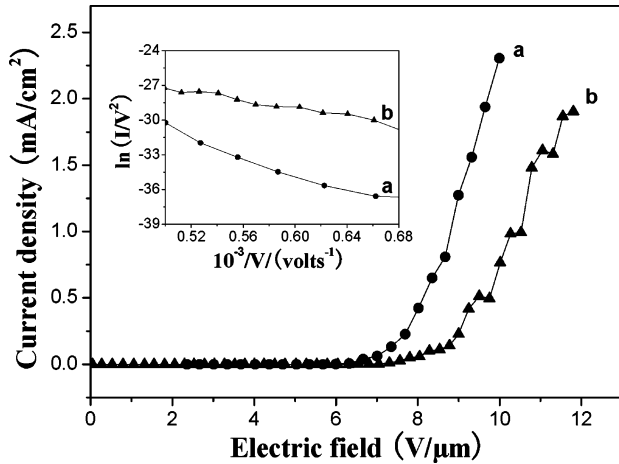


**Figure 4.** Typical FE current densities versus electric field curves for the  $V_2O_5 \cdot nH_2O$  nanorod arrays (the inset is the corresponding FN plots): (a) nanorod arrays without heat treatment and (b) ones with heat treatment.

and (d) the gravity action, hindering the synthesis. It is under these combined forces that  $V_2O_5 \cdot nH_2O$  nanorod arrays have formed. Every time, while pumping, beneficial aspects (a, b, and c) for growth are dominant so that sols are lifted into the pores and adsorbed onto the walls of pores; after vacuum pumping, all of the forces (a, b, c, and d) will reach equilibrium, and the sols will be kept on the walls of the pores. Repetition goes on, and after many times (here, more than three times) of pumping, the pores are filled with the sols. Then, while drying, a small amount of  $O_2$  discontinuously emits out of the sols, which makes the adhesion between the pore walls and the filling material sols weak. Therefore, according to the principles of shrinkage and densification,<sup>16</sup> eventually, the solid one-dimensional nanostructures are achieved. This mechanism is different from the one of fabrication of  $V_2O_5$ - $TiO_2$  composite nanorod arrays.<sup>7</sup> We thought that the growth of our samples started on the walls of the pores and continued along the radial direction until the solid nanostructures formed. In other words, the formation of the one-dimensional nanostructures was from the peripheral to the center, from hollow to solid, and from bottom to top because of the pulling effect of negative pressure. Therefore, this mechanism indicates that we can obtain a configuration of hollow nanostructure if we control the appropriate process parameters. As a matter of fact, we have successfully fabricated  $V_2O_5 \cdot nH_2O$  nanotube arrays by this method.<sup>2</sup> Compared with the previous method,<sup>7</sup> this method is helpful and time-saving because the vacuum pumping accelerates the filling of pores, especially for smaller diameter pores. Meanwhile, the smaller the evaporation area, the slower the evaporation. The diameters of the pores of the templates that we used are 200 nm, smaller than ones (400 nm) that others adopted.<sup>7</sup> Our early experiments show that, only depending on the capillary force, without the help of negative pressure, no evident one-dimensional nanostructures appeared even though aging occurred for more than 24 h. Thus, we consider that the negative pressure plays a key role for the growth. In addition, our processing method is generally applicable to synthesizing nanostructures of other oxides.<sup>19</sup>

The plots of the emission current densities versus the electric field for the as-synthesized samples (a) before and (b) after heat treatment with the same emitting surface area of  $7.85 \text{ mm}^2$  are shown in Figure 4. Their electron emission turn-on fields ( $E_{10}$ ), defined as the macroscopic fields required to produce a current density of  $10 \mu\text{A}/\text{cm}^2$ , are about 6.37 and  $7.31 \text{ V}/\mu\text{m}$ ,

**TABLE 1: Comparison of FE Properties of the As-Synthesized Products**

	type	$d/$ $\mu\text{m}$	$R_{\text{tip}}/$ nm	$d/R_{\text{tip}}/$ $10^3$	$I_{\text{max}}/$ ( $\text{mA}/\text{cm}^2$ )	$E_{10}/$ ( $\text{V}/\mu\text{m}$ )
$V_2O_5 \cdot nH_2O$	nanorod array <sup>a</sup>	300	125.70	2.39	2.31	6.37
$V_2O_5 \cdot nH_2O$	nanorod array <sup>b</sup>	200	81.87	2.44	1.90	7.31

<sup>a</sup> Before heat treatment. <sup>b</sup> After heat treatment.

respectively. In general, according to the standard of the Samsung Corporation, the emission current density for industrial video graphics array field emission displays (VGAFED) is  $1 \text{ mA}/\text{cm}^2$ . Here, their maximum emission current densities ( $I_{\text{max}}$ ) of the present vanadium oxide nanorod arrays are 2.31 and  $1.90 \text{ mA}/\text{cm}^2$  at the fields of 10.00 and  $11.81 \text{ V}/\mu\text{m}$ , respectively.

It is known that at room temperature, the emission current mainly originates from the tunneling of electrons through the surface barrier, which is described by the Fowler–Nordheim (FN) theory.<sup>20</sup> The FN equation can be expressed as

$$I = E_{\text{loc}}^2 \exp(-6.8 \times 10^7 \Phi^{3/2} / E_{\text{loc}}) \quad (1)$$

where  $I$  is the current density,  $E_{\text{loc}}$  is the local electric field nearby the emitter tip, and  $\Phi$  is the work function of the  $V_2O_5$  nanorods. For an isolated hemisphere model

$$E_{\text{loc}} = \frac{V}{\alpha R_{\text{tip}}} \quad (2)$$

where  $V$  is the applied field,  $R_{\text{tip}}$  is the tip radius of curvature, and  $\alpha$  is a modifying factor. Combining eqs 1 and 2, we obtain

$$\ln\left(\frac{I}{V^2}\right) = \frac{1}{V}(-6.8 \times 10^7 \alpha R_{\text{tip}} \Phi^{3/2}) + \text{offset} \quad (3)$$

The FN plots of  $(\ln I/V^2)$  versus  $(1/V)$  are represented in the inset of Figure 4. It is interesting to reveal that the FN plots have a linear relationship with a one- or two-stage slope, which implies that the field emissions from the  $V_2O_5 \cdot nH_2O$  nanorod arrays follow the FN theory and the emitted currents are indeed caused by quantum tunneling.<sup>1,20</sup> The results indicate that the  $V_2O_5 \cdot nH_2O$  nanorod arrays can be promising candidates as FE emitters.

What's more, according to ref 21

$$E_{\text{loc}} = \beta E = \beta \frac{V}{d} \quad (4)$$

where  $\beta$  is the field enhancement factor and  $d$  is the distance between the sample and electrode. Combining eqs 2 and 4, a formula to estimate the field enhancement factor of emitter films can be derived as

$$\beta = \frac{1}{\alpha} \cdot \frac{d}{R_{\text{tip}}} \quad (5)$$

With the help of Table 1 and by substituting the  $d$  value in our measurements, the  $\alpha$  value (range of 1–10),<sup>22</sup> and the average  $R_{\text{tip}}$  value for the  $V_2O_5 \cdot nH_2O$  nanorod, the enhancement factor for the nanorod can be as high as  $2.44 \times 10^3$  (using an  $\alpha$  of 1), which reveals that the local electric field at the tip can be sharply strengthened due to the small radius of curvature of the tiny nanotip.

From another angle, considering the screening effect between adjacent emitters,  $E_{loc}$  can be expressed by Filip's model<sup>23</sup>

$$E_{loc} = s \frac{V}{R_{tip}} + (1 - s) \frac{V}{d} \quad (6)$$

where  $s$  is a parameter describing the degree of the screening effect, which ranges from 0 for very densely arranged emitters to 1 for a single one. Combining expression 4 with eq 6, another formula to estimate the field enhancement factor of emitter films can be derived as

$$\beta = 1 + s \left( \frac{d}{R_{tip}} - 1 \right) \cong 1 + s \frac{d}{R_{tip}} \quad (7)$$

Substituting the  $d$  value and the  $R_{tip}$  value, the enhancement factor for a single V<sub>2</sub>O<sub>5</sub>·nH<sub>2</sub>O nanorod is also as high as  $2.44 \times 10^3$ , consistent with the above result ( $2.44 \times 10^3$ ) based on eq 5. Combining eqs 5 and 7, we can obtain

$$s \cong \frac{1}{\alpha} \quad (8)$$

Using an  $\alpha$  of 1–10, the calculated  $s$  value is 0.1–1, within the range of 0–1. The parameter  $s$  implies that the screening effect plays an important role in the actual field-emission process from nanorod arrays. This can also be seen from the SEM image shown in Figure 2a, in which the V<sub>2</sub>O<sub>5</sub>·nH<sub>2</sub>O nanorods of high density cover the substrate, resulting in the domination of the screening effect in the field emission. It is expected that the field-emission properties will be improved significantly from V<sub>2</sub>O<sub>5</sub>·nH<sub>2</sub>O nanorods with relatively lower growth density. In any case, the performance of field emission from as-grown V<sub>2</sub>O<sub>5</sub>·nH<sub>2</sub>O nanorods is encouraging and promises great potential for future applications in flat-panel displays.

The comparison of FE properties of the as-synthesized products is shown in Table 1. Comparing the as-prepared nanorod arrays before heat treatment with ones after heat treatment, it can be clearly indicated that the former owns better FE properties: higher  $I_{max}$  and lower  $E_{10}$ . The reason for this phenomenon may be the differences for the microstructure and energy for the samples before and after heat treatment. It can be analyzed from two aspects, the nature and microstructure, corresponding to  $\Phi$  and  $\beta$ . First, it is the different crystallinity degrees of the samples, amorphous and crystalline, which represent the aspect of nature. Compared with the crystalline structure, the electrons in the amorphous structure suffer fewer binds, and it can be easier to obtain energies, which makes them easier to escape from the surface fields of the materials and get into the vacuum to become FE electrons. That corresponds to the smaller  $\Phi$ . Therefore, the former amorphous vanadium oxide has the advantage in FE behaviors. Second, regarding the aspect of microstructure, Table 1, one can compare the values of  $d/R_{tip}/10^3$  between the former and latter. The former has the lower value (2.39) of  $d/R_{tip}/10^3$ , but it closely approaches the latter (2.44). Moreover, considering the screening effect, without the support and isolation of the PC template (pores), the latter has relatively denser nanorods, giving rise to the lower  $s$  value.

Under the effects of  $d/R_{tip}$  and  $s$ , perhaps here  $s$  playing the main role, relatively, the value of  $\beta$  for the former is higher. Due just to the above combining effects, the former shows the better FE properties. In a word, these results demonstrate that the FE current is significantly effected by the forms and crystallinity degrees of the vanadium oxide samples, and the one-dimensional nanoarrays with higher aspect ratio and relatively lower growth density will possess better FE effects.

## Conclusions

Aligned V<sub>2</sub>O<sub>5</sub>·nH<sub>2</sub>O nanorods with an average tip radius of ~100 nm have been synthesized via a simple route of template-based physical wetting of V<sub>2</sub>O<sub>5</sub> sols. Low turn-on fields (6–8 V/ $\mu$ m), high maximum current densities (over 1 mA/cm<sup>2</sup>), and linear FN properties were determined on the prepared nanostructures and natures of the samples, opening up great possibilities in electron emitter and flat-panel display applications.

**Acknowledgment.** This work is financially supported by the National Natural Science Foundation of China (50672071, 50672072, 50702039, 50772085), the Key Project of MOE, China (105124), the Foundation for Innovation Research Team of Hubei Province (2005ABC004), and the Program for Changjiang Scholars and Innovative Research Team in University (IRT0547), MOE, China.

## References and Notes

- (1) Hsieh, C. T.; Chen, J. M.; Lin, H. H.; Shih, H. C. *Appl. Phys. Lett.* **2003**, *83*, 3383.
- (2) Zhou, C. W.; Mai, L. Q.; Liu, Y. L.; Qi, Y. Y.; Dai, Y.; Chen, W. *J. Phys. Chem. C* **2007**, *111*, 8202.
- (3) McIlroy, D. N.; Zhang, D.; Kranov, Y.; Norton, M. G. *Appl. Phys. Lett.* **2001**, *79*, 1540.
- (4) Pan, Z. W.; Dai, Z. R.; Wang, Z. L. *Science* **2001**, *291*, 1947.
- (5) Iijima, S. *Nature* **1991**, *354*, 56.
- (6) Martin, C. R. *Science* **1994**, *266*, 1961.
- (7) Takahashi, K.; Wang, Y.; Lee, K.; Cao, G. Z. *Appl. Phys. A* **2006**, *82*, 27.
- (8) Huczko, A. *Appl. Phys. A* **2000**, *70*, 365.
- (9) Wen, T. L.; Zhang, J.; Chou, T. P.; Limmer, S. J.; Cao, G. Z. *J. Sol-Gel Sci. Technol.* **2005**, *33*, 193.
- (10) Kyotani, T.; Tsai, L.; Tomita, A. *Chem. Mater.* **1996**, *8*, 2109.
- (11) Patrissi, C. J.; Martin, C. R. *J. Electrochem. Soc.* **1999**, *146*, 3176.
- (12) Wang, Y.; Takahashi, K.; Shang, H. M.; Cao, G. Z. *J. Phys. Chem. B* **2005**, *109*, 3085.
- (13) Takahashi, K.; Limmer, S. J.; Wang, Y.; Cao, G. Z. *J. Phys. Chem. B* **2004**, *108*, 9795.
- (14) Alnoso, B.; Livage, J. *J. Solid State Chem.* **1999**, *148*, 16.
- (15) Fontenot, C. J.; Wiench, J. W.; Pruski, M.; Schrader, G. L. *J. Phys. Chem. B* **2000**, *104*, 11622.
- (16) Wang, Y.; Cao, G. Z. *Chem. Mater.* **2006**, *18*, 2787.
- (17) Martin, C. R. *Acc. Chem. Res.* **1995**, *28*, 61.
- (18) Yu, H.; Chen, W.; Dai, Y.; Mai, L. Q.; Qi, Y. Y.; Peng, J. F. *J. Wuhan Univ. Technol., Mater. Sci. Ed.* **2006**, *21*, 38.
- (19) Wang, Y.; Takahashi, K.; Lee, K.; Cao, G. Z. *Adv. Funct. Mater.* **2006**, *16*, 1133.
- (20) Tang, Q.; Li, T.; Chen, X.; Yu, D.; Qian, Y. *Solid State Commun.* **2005**, *134*, 229.
- (21) Zhao, Q.; Xu, J.; Xu, X. Y.; Wang, Z.; Yu, D. P. *Appl. Phys. Lett.* **2004**, *85*, 5331.
- (22) Chen, Y.; Patel, S.; Ye, Y.; Shaw, D. T.; Guo, L. *Appl. Phys. Lett.* **1998**, *73*, 2119.
- (23) Filip, V.; Nicolaescu, D.; Tanemura, M.; Okuyama, F. *Ultramicroscopy* **2001**, *89*, 39.